Electronic Supplementary Material (ESI) for Nanoscale

Supporting information

Force Measurements on Natural Membrane Nanovesicles Reveal a Composition-Independent, High Young's modulus

Annalisa Calò[*], *David Reguera, Gerard Oncins, Marie-Annick Persuy, Guenhaël Sanz, Simona Lobasso, Angela Corcelli, Edith Pajot-Augy, Gabriel Gomila*

Morphological nanovesicles data

	h_{NV} (topography) (nm)	w_{NV} (nm)	h_{NV} (FC) (nm)	R_{NV} (nm)
Plasmatic NV	38	94	39 ± 5	48 ± 3
	24	97	23 ± 3	64 ± 6
	29	88	32 ± 2	47 ± 2
	21	193	49 ± 5	120 ± 6
	14	87	30 ± 3	47 ± 1
	21	153	25 ± 5	135 ± 22
	25	220	27 ± 2	241 ± 19
	55	294	56 ± 6	222 ± 19
	19	192	22 ± 5	233 ± 51

	h_{NV} (topography) (nm)	w_{NV} (nm)	h_{NV} (FC) (nm)	R_{NV} (nm)
Inner NV	19	64	19 ± 3	38 ± 4
	20	113	28 ± 3	73 ± 6
	47	190	60 ± 6	106 ± 5
	26	104	44 ± 2	53 ± 0.4
	30	169	44 ± 3	104 ± 5
	22	152	48 ± 8	85 ± 6
	19	141	23 ± 2	122 ± 10
	19	98	22 ± 3	66 ± 7
	14	106	16 ± 3	100 ± 20
	44	196	43 ± 9	136 ± 16
	37	282	38 ± 3	283 ± 22
	21	137	25 ± 3	109 ± 11

Table S1. Data of the nanovesicles geometry, extracted from both AFM topography and force spectroscopy experiments. Left panel is for nanovesicles from the plasma membrane fraction and right panel for nanovesicles from the inner membrane fraction. For each nanovesicle we report the height at the centre and the width as measured from topographic images, the height as measured from force spectroscopy curves and the radius of curvature assuming spherical cap geometry.

Immunoblot and TLC lipid analyses of membrane subfractions

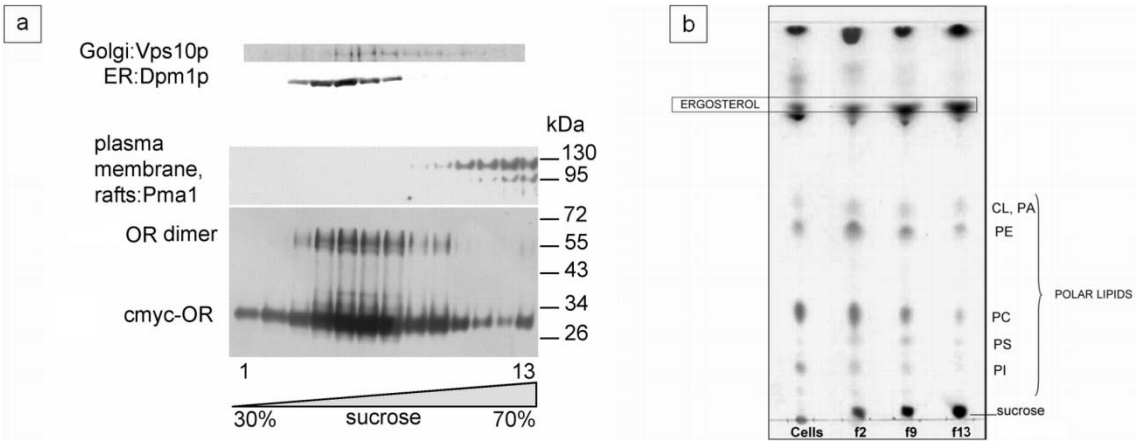

Figure S1. (a) Analysis of sucrose density gradient membrane subfractions by immunoblotting. (b) TLC lipid profiles of OR-containing membrane fractions. Total lipids were extracted from crude membranes of yeast cells expressing the OR and from various membrane subfractions separated by sucrose density gradient (fractions 2, 9 and 13). 40 µg of each lipid extract were loaded on each lane. Lane 1: yeast crude membranes, lane 2: fraction 2, lane 3: fraction 9, lane 4: fraction 13. (CL: cardiolipin, PA: phosphatidic acid, PE: phosphatidylethanolamine, PC: phosphatidylcholine, PS: phosphatidylserine, PI: phosphatidylinositol).

Pma1 is a yeast plasma membrane protein and a lipid raft marker. Figure S1a shows that it localizes in subfractions with the highest sucrose content (fractions 9-13). Fraction 2 does not contain lipid rafts and could be principally made up of membrane from vacuoles[1]. In order to characterize the membrane fractions of the engineered yeasts, the lipid composition of various sucrose density gradient subfractions was analyzed. Lipids were directly extracted from the sucrose fractions, without prior treatments to remove sucrose, to avoid loss of materials; as a consequence only a qualitative comparison of

TLC lipid profiles is possible. In particular, Figure S1b compares the TLC lipid profiles of yeast crude membranes and of some OR-containing membrane subfractions (fractions 2, 9 and 13). It can be seen that fractions 9 and 13 (rafts-containing membranes) and fraction 2 (membranes containing no rafts) have a qualitatively similar polar lipid composition, but different from that of whole membrane fraction. In all membrane fractions tested, PC, PE, PI and PS were the predominant glycerophospholipid classes. In particular the PC/PE and PI/PS ratios were close to 1 in both rafts containing subfractions and others, while in the lipid profiles of the whole membrane fraction, PC was more abundant than PE, and PI was more abundant than PS. Furthermore, a higher ergosterol-to-polar lipids ratio (i.e. ergosterol enrichment) was observed in the same rafts-containing subfractions than in fraction 2 or whole membrane fraction profiles.

Electrostatic contribution to the force curves

The force experienced by a charged tip approaching a charged surface can be described by the DLVO theory as a function of the tip-sample separation distance (D) as:

$$F(D) = \frac{4 \cdot \pi \cdot R_{tip} \cdot \lambda \cdot \sigma_{tip} \cdot \sigma_{NV}}{\varepsilon} e^{-D/\lambda} \qquad \text{Eq. S1}$$

where R is the tip curvature radius, λ the Debye length of the medium, σ_{tip} and σ_{NV} the surface charge density of the tip and the sample respectively and ε the dielectric constant of the medium (in the case of PBS $\varepsilon = 78$[2]).

In order to estimate the electrostatic DLVO contribution to the experimental force curves we experimentally measured the ζ-potential of a batch of nanovesicles from the total membrane fraction of *Saccharomyces cerevisiae*[3] and estimated their surface charge from the Grahame equation:

$$\sigma_{NV} \cong \varepsilon_0 \cdot \varepsilon \cdot \lambda^{-1} \cdot \zeta = -5.49 \cdot 10^{-3}\, C/m^2 \qquad \text{Eq. S2}$$

where ε_0 is the vacuum permittivity and ζ is the ζ-potential. The Debye length of the PBS solution 10 mM (ionic strength = 160.7 mM) is $7.59 \cdot 10^{-10}$ m and the surface charge density of the probe was measured according to the method reported by Drelich et al.[4,5], giving σ_{tip} = -0.04 C/m^2. Figure S2 shows the electrostatic force F vs. distance D. In the very few nanometers before the tip-sample contact the variation of the force due to their electrostatic repulsion is in the tens of pN range well below the nN range measured in the nanomechanical experiments.

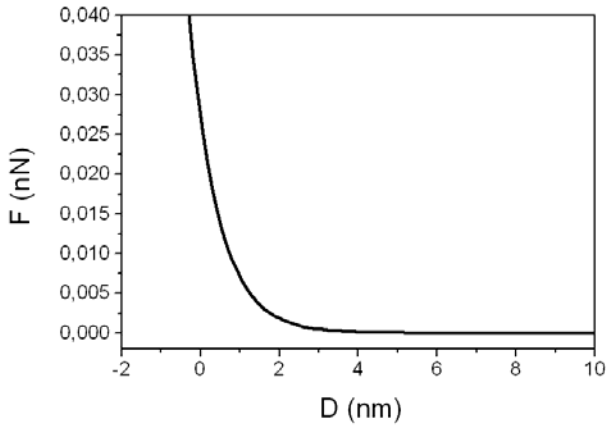

Figure S2. Evolution of the electrostatic force vs. tip-sample separation distance D according to Supplementary equation 1.

Verification of the thin shell model in the case of nanovesicles indentation by finite elements simulations

In order to verify the scaling predicted by the thin shell theory (and expressed in Eq. 2) and to extract a reliable value of the Young's modulus as an intrinsic property of the nanovesicles which is not dependent on their geometry, we performed finite elements simulations of the indentation of nanovesicles with different geometrical characteristics. In all cases, the nanovesicles are assumed to be adsorbed on the substrate, adopting a nearly spherical cap shape, as shown in Figure 3b.

Figure S3a shows the force curves obtained for a nanovesicle of h_{NV} = 30 nm, w_{NV} = 120 nm, E = 200 MPa, indented on a hard substrate by a spherical tip with R_{tip} = 9 nm, as a function of the thickness of its shell t in the range 1 to 10 nm. When the force curves are rescaled by t^2, as predicted by the thin shell model, a reasonably good collapse in the initial linear region is obtained (see Figure S3b). The curves deviate from this collapse in the deformation region corresponding to inverse buckling, which roughly occurs for indentations higher than the shell thickness.

Figure S4a shows the force curves obtained for a nanovesicle with the same R_{tip}, h_{NV} and E values (t = 5 nm), indented on a hard substrate, for different values of the width w_{NV} in the range 60-200 nm. When the force curves are rescaled by the inverse of the radius of curvature R_{NV} (see Eq. 1 and 2), a very good collapse in the initial linear region is obtained as predicted by thin shell theory (see Figure S4b). Thus, despite the fact that the finite elements simulations are not based on a specific assumption of an interpretative model, i.e. on the thin shell approximation, the resulting F vs. δ curves at low indentations follow the same dependency on t, E, h_{NV} and w_{NV}, as it is predicted by Eq. 1 and 2.

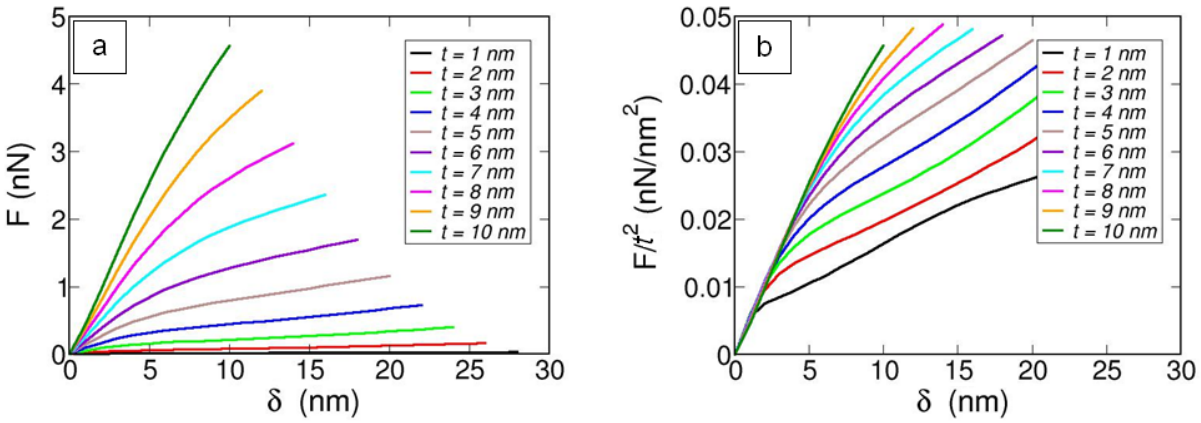

Figure S3. F vs. δ curves for a nanovesicle of h_{NV} = 30 nm, w_{NV} = 120 nm, E = 200 MPa, with different t indicated in the legend (a). F/t^2 reported vs. δ for the same shell thicknesses (b).

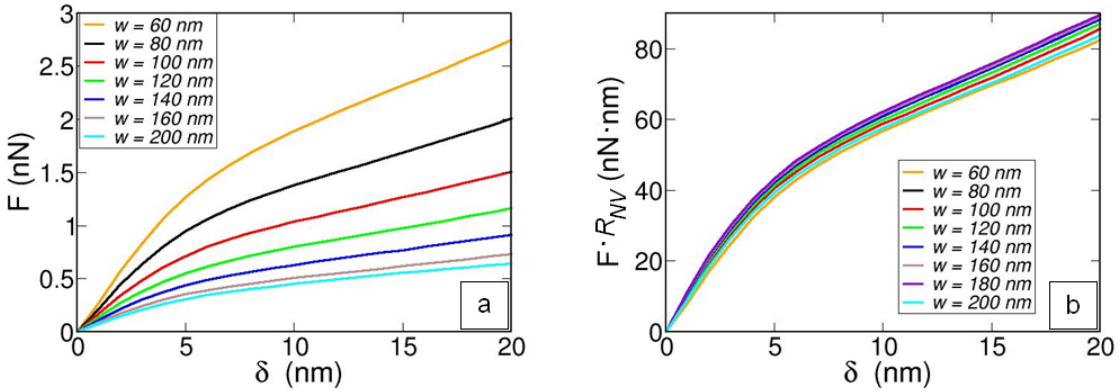

Figure S4. Force vs. δ curves for a nanovesicle of h_{NV} = 30 nm, t = 5 nm, E = 200 MPa, with different widths w_{NV} indicated in the legend (a). F multiplied by the curvature radius R_{NV} vs. δ for the same shell widths (b).

References

1. Dupré, S., Haguenauer-Tsapis, R. Deubiquitination step in the endocytic pathway of yeast plasma membrane proteins: crucial role of doa4p ubiquitin isopeptidase. *Mol. Cell. Biol.* **21,** 4482-4494 (2001).

2. Malleo, D., Tanner Nevill, J., Lee, L. P., Morgan, H. Continuous differential impedance spectroscopy of single cells. *Microfluid. Nanofluid.* **9**, 191-198 (2010).

3. Calò, A. et al. Diffusion-controlled deposition of natural nanovesicles containing G-protein coupled receptors for biosensing platforms. *Soft Matter* **8**, 11632-11643 (2012).

4. Drelich, J., Long, J., Yeung, A. Determining Surface Potential of the Bitumen-Water Interface at Nanoscale Resolution using Atomic Force Microscopy. *Can. J. Chem. Eng.* **85,** 625-634 (2007).

5. Redondo-Morata, L., Oncins, G., Sanz, F. Force Spectroscopy Reveals the Effect of Different Ions in the Nanomechanical Behavior of Phospholipid Model Membranes: The Case of Potassium Cation. *Biophys. J.* **102,** 66-74 (2012).